ORIGINAL ARTICLE

Open Access

City-Bus-Route Demand-based Efficient Coupling Driving Control for Parallel Plug-in Hybrid Electric Bus

Qin-Pu Wang[1], Chao Yang[2] , Ya-Hui Liu[2]* and Yuan-Bo Zhang[2]

Abstract

Recently, plug-in hybrid electric bus has been one of the energy-efficient solutions for urban transportation. However, the current vehicle efficiency is far from optimum, because the unpredicted external driving conditions are difficult to be obtained in advance. How to further explore its fuel-saving potential under the complicated city bus driving cycles through an efficient control strategy is still a hot research issue in both academic and engineering area. To realize an efficient coupling driving operation of the hybrid powertrain, a novel coupling driving control strategy for plug-in hybrid electric bus is presented. Combined with the typical feature of a city-bus-route, the fuzzy logic inference is employed to quantify the driving intention, and then to determine the coupling driving mode and the gear-shifting strategy. Considering the response deviation problem in the execution layer, an adaptive robust controller for electric machine is designed to respond to the transient torque demand, and instantaneously compensate the response delay and the engine torque fluctuation. The simulations and hard-in-loop tests with the actual data of two typical driving conditions from the real-world city-bus-route are carried out, and the results demonstrate that the proposed method could guarantee the hybrid powertrain to track the actual torque demand with 10.4% fuel economy improvement. The optimal fuel economy can be obtained through the optimal combination of working modes. The fuel economy of plug-in hybrid electric bus can be significantly improved by the proposed control scheme without loss of drivability.

Keywords: Hybrid electric vehicle, Single-shaft parallel electromechanical powertrain, Coupling driving mode, Adaptive robust control

1 Introduction

As representative of new energy vehicles, plug-in hybrid electric vehicle is always a hot topic in the field of recent vehicle technology [1]. Especially in areas of urban public transport, the excellent performance of low energy consumption and low emissions makes the plug-in hybrid electric bus (PHEB) become the primary solution [2, 3]. Recently, with the application of the idle-stop technology [4], the all-electric range of PHEB might be extended by utilizing more pure electric driving [5]. Considering the traffic congestion in the big city of China,

the vehicle launch and accelerating condition might frequently appear in the driving cycles of the city bus [6]. However, in most cases the electric energy stored in the PHEB might not cover the whole city-bus-route, the optimal coordinated operation between the engine and the electric machine (EM) is very worthy of study [7]. Because of the configuration features, the coordinated control becomes very difficult especially for the single-shaft parallel hybrid powertrain with the automated mechanical transmission (AMT) [8–10]. To solve this problem, several solutions have been presented for real-time optimization of the steady-state energy flows utilizing dynamic programming presented by Li et al. [11] and Lin et al. [12], equivalent consumption minimization strategy presented by Yang et al. [13] and Geng et al. [14], or model predictive control (MPC) strategy presented by

*Correspondence: liuyahui@tsinghua.edu.cn
[2] State Key Laboratory of Automotive Safety and Energy, Tsinghua University, Beijing 100084, China
Full list of author information is available at the end of the article

Wang *et al. Chin. J. Mech. Eng.* (2018) 31:58

Page 2 of 11

Yan et al. [15]. Nevertheless, the transient process, such as the complicated electromechanical coupling working mode and the multi-modes transition, was not considered in these control strategies.

During a vehicle launch and accelerating process, PHEB might fulfill an electromechanical coupling-driving mode after a pure electric driving mode to ensure the operation efficiency until the engine torque satisfies the demand torque on a high efficient zone [16–18]. Therefore, the coupling driving mode, which refers to the hybrid driving mode or the engine active charging mode, is crucial for the vehicle launch and accelerating process of PHEB [16].

Considering the difference between dynamic characteristics of the engine and the EM, it is necessary to further study the coordinated control method for an efficient solution of the hybrid powertrain. Therefore, a novel torque-demand control approach based on the MPC was proposed by He et al. [19], to implement the torque control of parallel hybrid powertrain. In addition, for a parallel hybrid powertrain, the coordinated control method using dynamic input allocation, MPC, and sliding mode control method presented by Cordiner et al. [20], Minh et al. [21], and Metin et al. [22], respectively. Using the fast response behavior of the EM, an electromechanical coupling driving control scheme was proposed by Yang et al. [23, 24] to achieve good torque tracking performance.

The coordinated control strategies can ensure the torque tracking performance during a coupling driving process. However, the instantaneous variation of the traffic flows, road conditions, and the passenger loads in a city-bus-route, might greatly affect the robustness of the control system. To adaptively deal with the stochastic driving intention, a city-bus-route demand-based coupling driving control approach is designed for the single-shaft parallel PHEB with AMT. Firstly, the time-varying driving intention is quantified with a fuzzy logic, and then the coupling driving mode and the AMT gear-shifting strategy are determined with a strategy determination module. Secondly, considering the dynamic characteristics of the EM, the adaptive robust controller is designed for the EM to respond to the transient torque demand. Meanwhile, the response deviation and the transient fluctuation of the engine torque are compensated with the fast response behavior of the EM.

The rest of the paper is organized as follows: Section 2 gives the models of the single-shaft parallel PHEB. The efficient coupling driving control approach is developed in Section 3. The results of simulation and hard-in-loop (HIL) test are given in Section 4. Finally, the conclusion and discussion are given in Section 5.

2 Model Descriptions

A typical single-shaft parallel hybrid powertrain is illustrated as Figure 1.

As shown in Figure 1, the EM is placed between the output of clutch and the input of AMT, and the clutch could implement the mode transition of this powertrain with engagement and disengagement operations. AMT could assist the vehicle to adapt to the demand from different conditions, and help the engine and the EM to work in their efficient zones as well. Furthermore, the parameters of the studied PHEB are shown in Table 1.

2.1 Energy Demand Analyses of City Bus Route

During the operation, PHEB with that powertrain could fulfil six basic working modes, including idling stop mode, pure electrical driving mode, engine driving mode, hybrid driving mode, engine active charging mode, and regenerative braking mode. The diagram of the PHEB energy demand corresponded to the working modes mentioned above is shown in Figure 2. As shown in Figure 2, between two bus stops, the expected engine operation in PHEB might contain two states, engine-off and engine high-efficiency operation. The engine-off state occurs at the idling stop mode, pure electrical driving mode, and the regenerative braking mode. With the increasing driving demand torque the engine will be started and engaged into the driveline. Then the problem of fuel saving becomes the optimization problem of engine working points. It should be noted that the EM might be utilized to assist the engine running in its high-efficiency area both in the hybrid driving mode and the engine active charging mode. Thus, those two modes are very important for improving the fuel economy of PHEB.

2.2 Diesel Engine Model

The simplified model of the diesel engine is employed for the torque control, which could be shown in Figure 3.
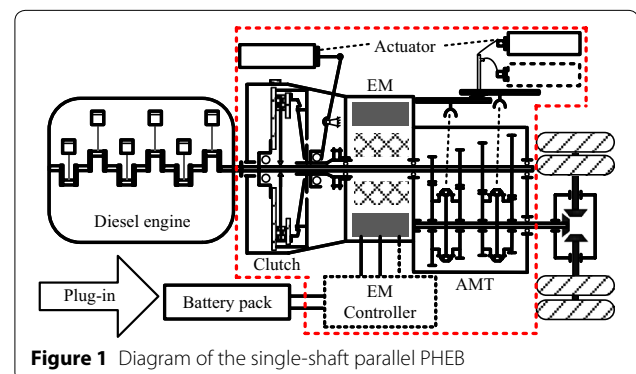

Figure 1 Diagram of the single-shaft parallel PHEB

Wang *et al. Chin. J. Mech. Eng.* (2018) 31:58

Page 3 of 11

Table 1 Parameters of HEB powertrain

Components	Description
Diesel engine	YC6J200-42, nominal power: 147 kW
EM	Permanent magnet, max torque: 750 Nm, nominal power: 94 kW, peak power: 121 kW
Battery	Lithium titanate battery, capacity: 60 Ah, nominal voltage: 346 V
Gearbox	AMT, gear ratios: 7.05, 4.13, 2.52, 1.59, 1, 0.78. Efficiency of gearbox is assumed 95%
Final drive ratio	4.2
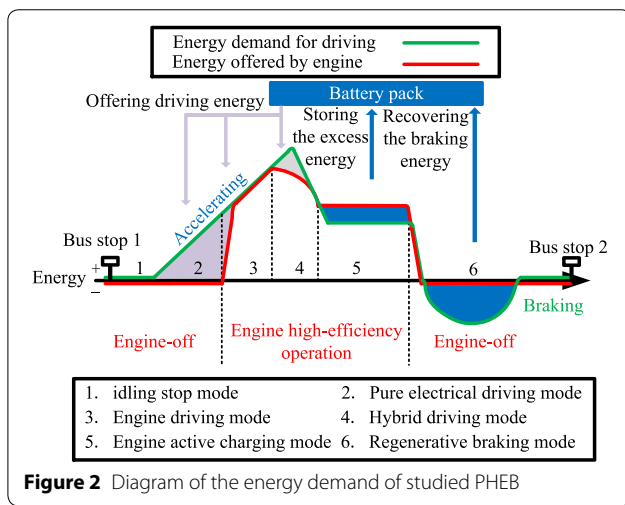
Figure 2 Diagram of the energy demand of studied PHEB
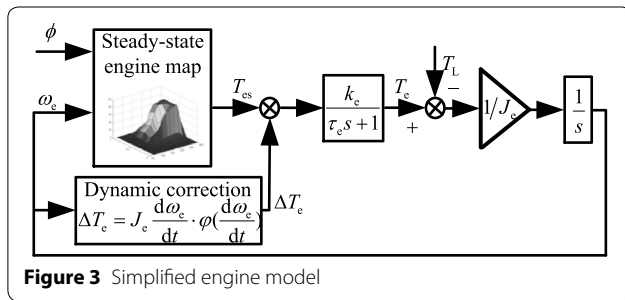
Figure 3 Simplified engine model

In Figure 3, ϕ represents the accelerator pedal position. J_e is the moment of inertia of the crankshaft; ω_e is the rotational speed of the crankshaft; $\varphi(\mathrm{d}\omega_e/\mathrm{d}t)$ is the dynamic compensation factor; k_e and τ_e are the proportional coefficient and the time constant, respectively; T_e and T_L are the effective torque and the load torque of the engine, respectively; T_{es} is the static torque of the engine, which could be obtained from the engine map; ΔT_e represents a dynamic correction item of the engine torque, which could be described as follows:

$$\Delta T_e = J_e \frac{\mathrm{d}\omega_e}{\mathrm{d}t} \cdot \varphi\left(\frac{\mathrm{d}\omega_e}{\mathrm{d}t}\right). \tag{1}$$

Only considering the rotational dynamics of the crankshaft, the engine model could be written as follows:

$$\begin{cases} J_e \dot{\omega}_e = T_e - T_L, \\ T_e = T_{es} - \Delta T_e - f_1(\mathrm{d}\phi/\mathrm{d}t). \end{cases} \tag{2}$$

2.3 EM Model

The control-oriented dynamic model of the EM consists of two modes: the driving mode and the generating mode. In order to realize the transient torque tracking control, the axis models are employed, when the EM operates in the driving mode:

$$\begin{cases} \frac{\mathrm{d}\omega_m}{\mathrm{d}t} = \frac{1}{J_m}T_m - \frac{B_\mu}{J_m}\omega_m - \frac{1}{J_m}T_l, \\ \frac{\mathrm{d}i_d}{\mathrm{d}t} = -\frac{R_s}{L}i_d + P\omega_m i_q + \frac{1}{L}u_d, \\ \frac{\mathrm{d}i_q}{\mathrm{d}t} = -\frac{R_s}{L}i_q - P\omega_m i_d - \frac{P\Phi}{L}\omega_m + \frac{1}{L}u_q. \end{cases} \tag{3}$$

When the EM operates in the generating mode:

$$\begin{cases} \frac{\mathrm{d}\omega_m}{\mathrm{d}t} = \frac{1}{J_m}T_e - \frac{1}{J_m}T_m - \frac{B_\mu}{J_m}\omega_m - \frac{1}{J_m}T_l, \\ \frac{\mathrm{d}i_d}{\mathrm{d}t} = -\frac{R_s}{L}i_d + P\omega_m i_q - \frac{1}{L}u_d, \\ \frac{\mathrm{d}i_q}{\mathrm{d}t} = -\frac{R_s}{L}i_q - P\omega_m i_d + \frac{P\Phi}{L}\omega_m - \frac{1}{L}u_q, \end{cases} \tag{4}$$

where i_d and i_q are the d and q axis stator currents, respectively; u_d and u_q are the d and q axis stator voltages, respectively; R_s, L, P and Φ represent the stator resistance, the stator inductance, the number of the pole pairs, and magnet's flux linkage, respectively; J_m and B_μ are the moment of inertia of the EM output shaft and the damping coefficient, respectively; T_e is the engine torque when the PHEB runs in the active charging mode, and T_m is the EM torque, which can be described as the following equation:

$$T_m = \frac{3}{2}P\Phi i_q. \tag{5}$$

3 City-Bus-Route Demand-based Efficient Coupling Driving Control Strategy

In this section, a novel city-bus-route demand-based coupling driving control strategy is presented. Firstly, the fuzzy logic controller quantifies the driver's driving intention. Then the AMT gear-shifting strategy and the coupling driving mode are determined with the quantified driving intention in the strategy determination module. Secondly, the designed PI controller for engine and adaptive robust controllers for EM implement the torque tracking control in the coupling driving mode. Moreover,

Wang *et al. Chin. J. Mech. Eng.* (2018) 31:58

Page 4 of 11

considering the properties of the single-shaft parallel hybrid powertrain, the response error of engine torque is compensated by the accurate EM torque control to guarantee the torque tracking performance of powertrain.

3.1 Fuzzy Logic Inference for Driving Intention

The driving intention is generated from the driver's maneuvers during the PHEB accelerating process. However, it is difficult to describe the intention accurately by the mathematical expressions. Therefore, the fuzzy logic based on the test data and experience is adopted to implement the quantification of the driving intention. Diagram of the fuzzy logic controller is shown in Figure 4.

As shown in Figure 4, the input variables are vehicle speed v_{veh}, the relative accelerator pedal position ϕ_{rel}, and the absolute value of the change rate of accelerator pedal position $d\phi/dt$, the output variable is driving intention I_d. The relative accelerator pedal position could be obtained by the equation as follows:

$$\phi_{rel} = \frac{100 \times (\phi - \phi_{equ})}{\phi_{equ}}, \tag{6}$$

where ϕ is actual accelerator pedal position, ϕ_{equ} is equilibrium accelerator pedal position reflecting the accelerator pedal position which maintains the vehicle driving on flat road with a uniform speed, and the value of ϕ_{equ} might be obtained through looking up the steady-state table with the inputs of the engine torque and the engine rotational speed, and the engine torque could be obtained by the vehicle longitudinal dynamics equation as follows:

$$T_e = (F_f + F_w)r / \eta_T i_g i_f, \tag{7}$$

where F_f and F_w are the rolling resistance and the aerodynamic drag, respectively. r, η_T, i_g, and i_f are wheel radius, transmission efficiency, AMT gear ratio, and differential ratio, respectively.

According to the test data of actual vehicle, the fuzzy logic rule base shown in Table 2 can be obtained. In Figure 5, the memberships of v_{veh} are L, M, and H, which represent the low speed,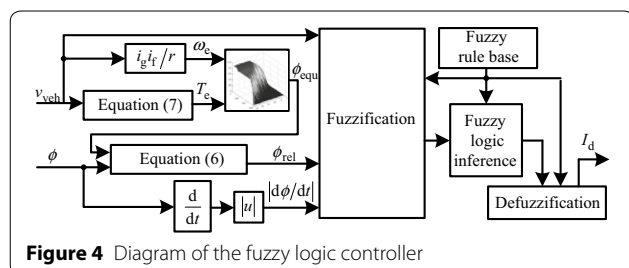 the middle speed, and the high speed, respectively. The memberships of f_{rel} are Nb, Ns, Z, Ps, and Pb, which are the negative big, the negative small, the zero, the positive small, and the positive big of the equilibrium accelerator pedal open, respectively. The memberships of df/dt are S, Mi, and Bi, which are the small, the middle, and the big of the change rate of accelerator pedal open, respectively. Moreover, the output variable I_d obtained by the defuzzification are quantified as St, D, K, A, and B, which represent the intention of stop, decelerating, keep, accelerating, urgent accelerating.

3.2 Balanced AMT Gear-shifting Strategy and Driving Mode Determination Module
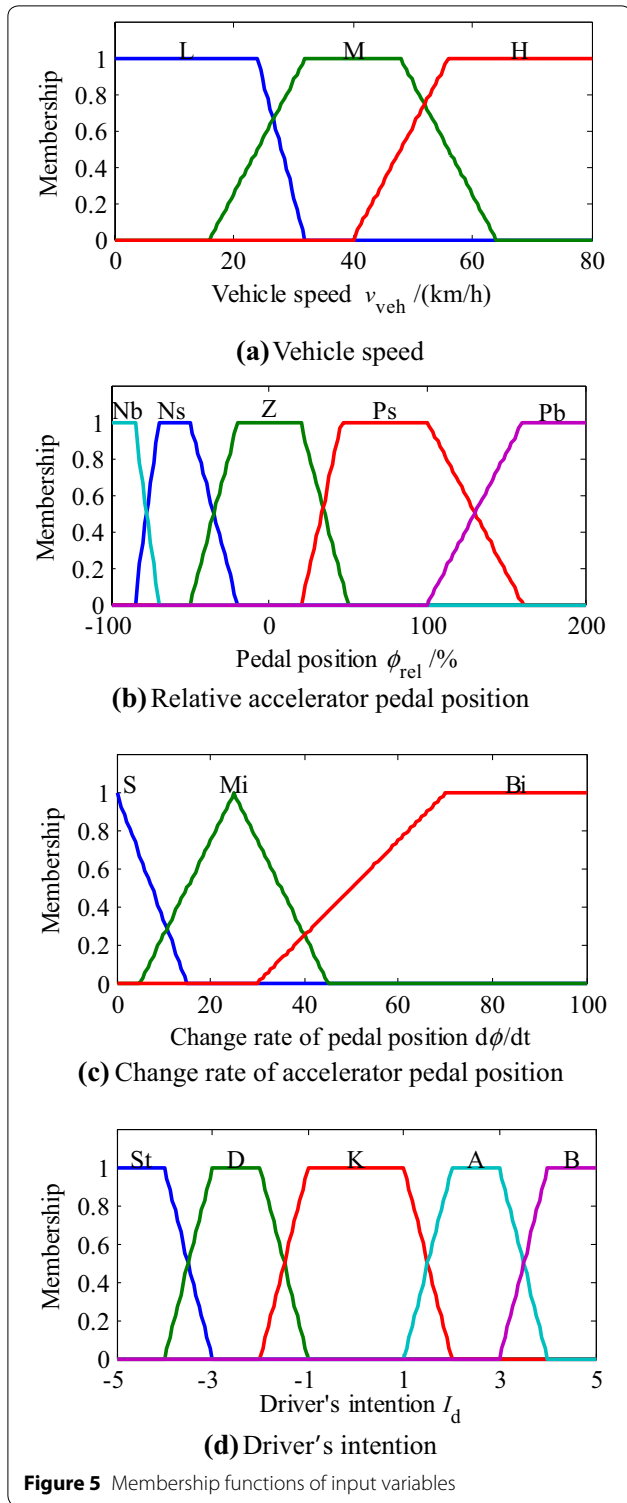
The double-parameters balanced AMT gear-shifting strategy (BGS), which balances the dynamic gear-shifting (DGS) maneuver and the economic gear-shifting (EGS) maneuver, is employed. This strategy tends to dynamic or economic depending on the driving intention, which could be quantified by the designed fuzzy inference. Taking the effects of engine operating points for example, the full DGS ensures that engine might work on the external characteristic line, and the full EGS reflects that engine would work on the optimal operating line with the highest efficiency. According to the quantified driving intention, the AMT gear-shifting maneuver might be determined that the gear-shifting maneuver tends to DGS with urgent accelerating intention and conversely tends EGS with keep and normal accelerating intention. Therefore, the energy-efficient operation of PHEB without drivability loss might be fulfilled by the proposed gear-shifting strategy.

Figure 4 Diagram of the fuzzy logic controller

Table 2 Fuzzy logic rule base

Relative pedal open φ_{rel}	Change rate of accelerator pedal position $d\varphi/dt$	Vehicle speed v_{veh}(km/h)		
		S	M	H
Nb	S	St	D	D
	Mi	St	D	D
	Bi	St	D	D
Ns	S	St	K	K
	Mi	St	D	D
	Bi	St	D	D
Z	S	St	St	K
	Mi	St	K	K
	Bi	St	K	K
Ps	S	A	K	K
	Mi	A	A	A
	Bi	B	B	B
Pb	S	A	A	A
	Mi	A	A	A
	Bi	B	B	B

Wang *et al. Chin. J. Mech. Eng.* (2018) 31:58

Page 5 of 11

(a) Vehicle speed

(b) Relative accelerator pedal position

(c) Change rate of accelerator pedal position

(d) Driver's intention

Figure 5 Membership functions of input variables

Combined with the quantified driving intention, the AMT gear-shifting strategy and the mode selection during the coupling driving mode can be determined, the logic of which is shown in Figure 6. In Figure 6, $I_d(t_{switch})$

is the driving intention when the engine engages into the driveline at the time t_{switch}, and I_{th} represents the logic threshold of driving intention, and its value could be obtained by repeated tests.

According to the description of PHEB working modes, the coupling driving modes can ensure the efficient operation of PHEB. As shown in Figure 7, the engine working points are improved into its high-efficiency area by EM in the coupling driving modes. However, during the simultaneous operation of engine and EM, the difference of dynamic characteristics between the engine and the EM causes the torque deviation of powertrain, which might significantly influence the drivability of PHEB. In this paper, the coordinated control scheme utilizes the EM to compensate the torque response deviation. Thus, the EM controller is very important that some uncertainties should be taken into account in the controller design. Then the design of the torque controllers for the engine and EM will be given in the next two parts.

3.3 PI torque Controller for Diesel Engine

In order to response the demand torque, a PI torque controller is designed. The expression can be written as:

$$u_{eng} = k_p\left(T_e^r - T_e\right) + k_i \int \left(T_e^r - T_e\right) dt, \qquad (8)$$

where u_{eng} is the engine control input that represent the fuel injection quantity, T_e^r is demand powertrain speed, k_p, k_i are proportional and integral gains, respectively.

3.4 Adaptive Robust Controllers for the EM Torque Tracking Control

To ensure the torque balance of the whole powertrain, the EM control system design might become the chief task. Then the objective of EM controller becomes that ensures the accurate trajectory tracking control with the existence of model uncertainties and external disturbances. First, the error models of EM in the driving mode and generating mode are necessary. Therefore, the error variables can be defined as follows:

$$\begin{aligned}
\boldsymbol{x} &= \begin{bmatrix} x_1 & x_2 & x_3 \end{bmatrix}^T \\
&= \begin{bmatrix} \omega_m - \omega_m^r & i_d - i_d^r & i_q - i_q^r \end{bmatrix}^T, \\
\bar{\boldsymbol{x}} &= \begin{bmatrix} \bar{x}_1 & \bar{x}_2 & \bar{x}_3 \end{bmatrix}^T \\
&= \begin{bmatrix} \omega_m - \omega_m^* & i_d - i_d^* & i_q - i_q^* \end{bmatrix}^T,
\end{aligned} \qquad (9)$$

where $\boldsymbol{x}$ and $\bar{\boldsymbol{x}}$ are the error variables when the EM works in the driving mode and generating mode, respectively. ω_m^r, i_d^r, i_q^r are the desired values of the EM speed, the
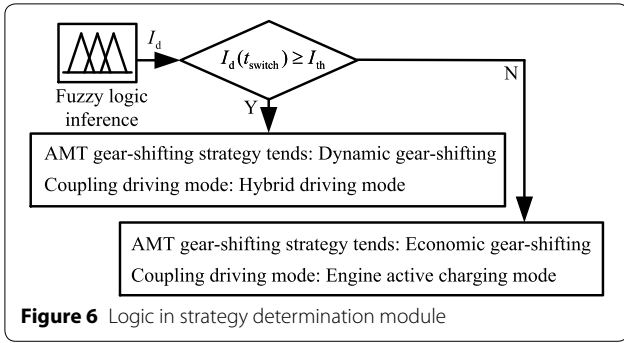
Wang *et al. Chin. J. Mech. Eng.* (2018) 31:58

Page 6 of 11

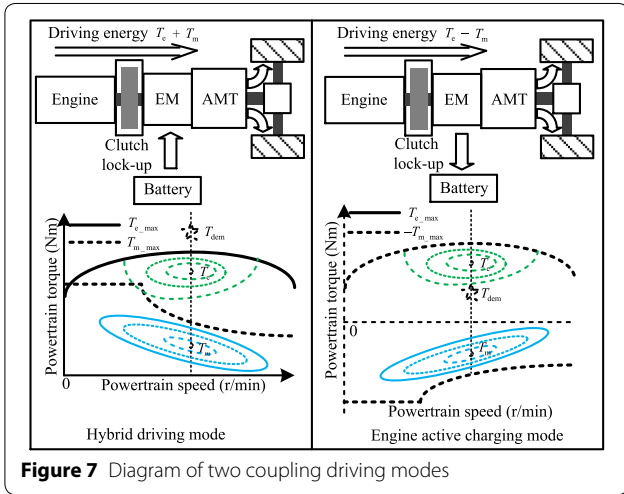**Figure 6** Logic in strategy determination module

Figure 7 Diagram of two coupling driving modes

d-axis, and the q-axis stator currents when the EM operates in the driving mode, respectively. ω_m^*, i_d^*, i_q^* are the desired values of the EM speed, the d-axis, and the q-axis stator currents when the EM operates in the generating mode, respectively. Combining with the EM model described in Eqs. (3) and (4), the error equations that have considered the uncertainties can be defined when EM operates in the driving mode:

$$\begin{cases} \dot{x}_1 = \frac{3P\Phi}{2J_m}x_3 - \theta_1 x_1 - \tilde{\theta}_1 \omega_m^r - w_1, \\ \dot{x}_2 = -\theta_2 x_2 + P(x_1 x_3 + x_1 i_q^r + \omega_m^r x_3) + u_1, \\ \dot{x}_3 = -\theta_2 x_3 - P(x_1 x_2 + \omega_m^r x_2) - \frac{P\Phi}{L}x_1 - \tilde{\theta}_2 i_q^r + u_2. \end{cases} \quad (10)$$

When EM operates in the generating mode:

$$\begin{cases} \dot{\bar{x}}_1 = T_E - \frac{3P\Phi}{2J_m}\bar{x}_3 - \tau_1 \bar{x}_1 - \tilde{\tau}_1 \omega_m^* - w_2, \\ \dot{\bar{x}}_2 = -\tau_2 \bar{x}_2 + P(\bar{x}_1 \bar{x}_3 + e_1 i_q^* + \omega_m^* \bar{x}_3) + u_3, \\ \dot{\bar{x}}_2 = -\tau_2 \bar{x}_3 - P(\bar{x}_1 \bar{x}_2 + \omega_m^* \bar{x}_2) + \frac{P\Phi}{L}\bar{x}_1 - \tilde{\tau}_2 i_q^* + u_4, \end{cases} \quad (11)$$

where the uncertainty parameters θ_1, θ_2, τ_1, and τ_2 are given as follows:

$$\begin{cases} \theta_1 = \frac{B_\mu}{J_m}, \theta_2 = \frac{R_s}{L}, \\ \tau_1 = \frac{B_\mu}{J_m}, \tau_2 = \frac{R_s}{L}, \end{cases} \quad (12)$$

$\tilde{\theta}_i$ and $\tilde{\tau}_i (i = 1, 2)$ are the error between the uncertain parameters and the adaptive estimated value, which would be described in later part. Moreover, w_1, w_2 represent the load disturbances of EM control system. Then the performance vectors are defined as follows:

$$\begin{cases} z = [\ \rho_1 x_1\ \ \rho_2 x_2\ \ \rho_3 x_3\ ]^{\mathrm{T}}, \\ \bar{z} = [\ \bar{\rho}_1 \bar{x}_1\ \ \bar{\rho}_1 \bar{x}_1\ \ \bar{\rho}_1 \bar{x}_1\ ]^{\mathrm{T}}, \end{cases} \quad (13)$$

where ρ_i and $\bar{\rho}_i$ ($i = 1, 2, 3$) are the weighting factors. T_E is an error term. Moreover, u_1, u_2, u_3, u_4 are equivalent control inputs described as follows:

$$\begin{cases} u_1 = P\omega_m^r i_q^r + \frac{1}{L}u_d, \\ u_2 = \hat{\theta}_2 i_q^r - \frac{P\Phi}{L}\omega_m^r - \dot{i}_q^r + \frac{1}{L}u_q, \end{cases} \quad (14)$$

$$\begin{cases} u_3 = P\omega_m^* i_q^* - \frac{1}{L}u_d, \\ u_4 = \tilde{\tau}_2 i_q^* + \frac{P\Phi}{L}\omega_m^* - \dot{i}_q^* - \frac{1}{L}u_q, \end{cases} \quad (15)$$

Then the control objective of EM controller becomes that the closed-loop system is stable with L_2-gain, that is, when $w \neq 0$, the system from the disturbance inputs w_i ($i = 1, 2$) to the penalty outputs z and $\bar{z}$ has finite L_2-gain not larger than γ_i ($i = 1, 2$).

$$\begin{cases} \int_0^T \|z(t)\|^2 \mathrm{d}t \leq \gamma_1 \int_0^T \|w_1(t)\|^2 \mathrm{d}t, \quad \forall w_1, \\ \int_0^T \|\bar{z}(t)\|^2 \mathrm{d}t \leq \gamma_2 \int_0^T \|w_2(t)\|^2 \mathrm{d}t, \quad \forall w_2, \end{cases} \quad (16)$$

where $T > 0$ is any given scalar. γ_i ($i = 1, 2$) are the evaluating factors. Thus, regarding the system described in Eqs. (10) and (11), an adaptive robust controller for EM is designed when EM operates in the driving mode:

$$\begin{cases} u_1 = \hat{\theta}_2 x_2 - P(x_1 x_3 + x_1 i_q^r + \omega_m^r x_3) - k_2 x_2, \\ u_2 = \left(\frac{P\Phi}{L} - \frac{3P\Phi}{2J_m}\right)x_1 + \hat{\theta}_2 x_3 + P(x_1 x_2 + \omega_m^r x_2) \\ \quad + \frac{\partial \alpha_1}{\partial x_1}\frac{3P\Phi}{2J_m}x_3 - \frac{\partial \alpha_1}{\partial x_1}\hat{\theta}_1 x_1 - \frac{\partial \alpha_1}{\partial x_1}\hat{\theta}_2 + \frac{\partial \alpha_1}{\partial \hat{\theta}_1}\dot{\hat{\theta}}_1 \\ \quad - \frac{1}{2\gamma_1^2}Z_1\left(\frac{\partial \alpha_1}{\partial x_1}\right)^2 - k_3 Z_1. \end{cases} \quad (17)$$

And the parameter adaptive update laws are chosen as

$$\begin{cases} \dot{\hat{\theta}}_1 = \chi_1\left(\frac{\partial \alpha_1}{\partial x_1}x_1 Z_1 - x_1^2 - \omega_m^r x_1 + \frac{\partial \alpha_1}{\partial x_1}\omega_m^r Z_1\right), \\ \dot{\hat{\theta}}_2 = \chi_2(-x_3 Z_1 - x_2^2 - i_q^r Z_1). \end{cases} \quad (18)$$

Wang *et al. Chin. J. Mech. Eng.* (2018) 31:58

Page 7 of 11

When EM operates in the generating mode:

$$
\begin{cases}
u_3 = \hat{\tau}_2 \bar{x}_2 - P(\bar{x}_1 \bar{x}_3 + \bar{x}_1 i_q^* + \omega_m^* \bar{x}_3) - \bar{k}_2 \bar{x}_2, \\
u_4 = \left(\frac{3P\Phi}{2J_m} - \frac{P\Phi}{L}\right)\bar{x}_1 + P(\bar{x}_1 \bar{x}_2 + \omega_m^* \bar{x}_2) \\
\quad + \hat{\tau}_2 \bar{x}_2 - \frac{P\Phi}{L}\bar{x}_1 + \frac{\partial \alpha_2}{\partial \bar{x}_1} T_E - \frac{\partial \alpha_2}{\partial \bar{x}_1}\frac{3P\Phi}{2J_m}\bar{x}_3 \\
\quad - \frac{\partial \alpha_2}{\partial \bar{x}_1}\hat{\tau}_1 \bar{x}_1 + \frac{\partial \alpha_2}{\partial \hat{\tau}_1}\dot{\hat{\tau}}_1 - \bar{k}_3 Z_2.
\end{cases}
\tag{19}
$$

And the parameter adaptive update laws are chosen as

$$
\begin{cases}
\dot{\hat{\tau}}_1 = \beta_1\left(\frac{\partial \alpha_2}{\partial \bar{x}_1}\bar{x}_1 Z_2 + \frac{\partial \alpha_2}{\partial \bar{x}_1}\omega_m^* Z_2 - \bar{x}_1^2 - \omega_m^* \bar{x}_1\right), \\
\dot{\hat{\tau}}_2 = \beta_2(-\bar{x}_3 Z_2 - \bar{x}_2^2 - i_q^* Z_2),
\end{cases}
\tag{20}
$$

where $k_i(i = 1, 2, 3)$ and $\bar{k}_i(i = 1, 2, 3)$ are adjustable parameters of the controller, $Z_1 = x_3 - \alpha_1(x_1, \hat{\theta}_1)$ and $Z_2 = \bar{x}_3 - \alpha_2(\bar{x}_1, \hat{\tau}_1)$, $\alpha_1(x_1, \hat{\theta}_1)$ and $\alpha_2(\bar{x}_1, \hat{\tau}_1)$ are virtual controllers which could be chosen as follows:

$$
\begin{cases}
\alpha_1(x_1, \hat{\theta}_1) = \frac{2J_m}{3P\Phi}\left(\hat{\theta}_1 x_1 - k_1 x_1 - \frac{1}{2\gamma_1^2}x_1\right), \\
\alpha_2(\bar{x}_1, \hat{\tau}_1) = \frac{2J_m}{3P\Phi}\left(T_E - \hat{\tau}_1 \bar{x}_1 + \bar{k}_1 \bar{x}_1 + \frac{1}{2\gamma_2^2}\bar{x}_1\right).
\end{cases}
\tag{21}
$$

In addition, $\chi_i(i = 1, 2)$ and $\beta_i(i = 1, 2)$ are adjustable parameters of adaptive laws. Taking the driving mode of EM for example, the adaptive robust controller described in Eqs. (17) and (18) might be designed by the close-loop system Lyapunov stability analysis. First, a positive definite Lyapunov function is defined as follows:

$$
V = \frac{1}{2}x_1^2 + \frac{1}{2}x_2^2 + \frac{1}{2}Z_1^2 + \frac{1}{2}\tilde{\theta}^{\mathrm{T}}\Gamma^{-1}\tilde{\theta}.
\tag{22}
$$

Then, its time derivative could be calculated as follows:

$$
\begin{aligned}
V = {} & x_1\left(\frac{3P\Phi}{2J_m}x_3 - \theta_1 x_1 - \tilde{\theta}_1 \omega_m^r - w_1\right) \\
& + x_2[-\theta_2 x_2 + P(x_1 x_3 + x_1 i_q^r + \omega_m^r x_3) + u_1] \\
& + Z_1[-\theta_2 x_3 - P(x_1 x_2 + \omega_m^r x_2) - \frac{P\Phi}{L}x_1 - \tilde{\theta}_2 i_q^r + u_2] \\
& - \frac{\partial \alpha_1}{\partial x_1}\left(\frac{3P\Phi}{2J_m}x_3 - \theta_1 x_1 - \tilde{\theta}_1 \omega_m^r - w_1\right) - \frac{\partial \alpha_1}{\partial \hat{\theta}_1}\dot{\hat{\theta}}_1].
\end{aligned}
\tag{23}
$$

Remark: For the external disturbance w_1, the inequality transform might be used which can be written as follows:

$$
\begin{cases}
-x_1 w_1 \leq \frac{1}{2\gamma_1^2}x_1^2 + \frac{\gamma_1^2}{2}w_1^2, \\
\frac{\partial \alpha_1}{\partial x_1}w_1 Z_1 \leq \frac{\gamma_1^2}{2}w_1^2 + \frac{1}{2\gamma_1^2}Z_1^2\left(\frac{\partial \alpha_1}{\partial x_1}\right)^2.
\end{cases}
\tag{24}
$$

Choosing the adaptive robust controller described in Eqs. (17) and (18), and combining Eq. (24), Eq. (23) might become as follows:

$$
\begin{aligned}
\dot{V} \leq {} & -\left(k_1 - \frac{1}{2}\rho_1\right)x_1^2 - \left(k_3 - \frac{1}{2}\rho_3\right)Z_1^2 \\
& - \left(k_2 - \frac{1}{2}\rho_2\right)x_2^2 + \gamma_1^2 w_1^2 - \frac{1}{2}z^{\mathrm{T}}z,
\end{aligned}
\tag{25}
$$

where the adjustable gains $k_i(i = 1, 2, 3)$ should satisfy the conditions as follows:

$$
k_1 \geq \frac{1}{2}\rho_1, k_2 \geq \frac{1}{2}\rho_2, k_3 \geq \frac{1}{2}\rho_3.
\tag{26}
$$

Therefore, combing with the LaSalle invariant set principle, it can be concluded that the designed controller can achieve the mentioned above control objectives. Because the adaptive controller described in Eqs. (19) and (20) for the generating mode of EM is deduced that is similar with that of the driving mode of EM, so the proof procedure will be omitted here.

4 Validation Results and Analysis

The simulation and HIL tests are performed on a single-shaft parallel PHEB in MATLAB/Simulink. Basic parameters are listed in Table 1. Moreover, control parameters in Table 3 are selected among all parameters obtained from repeatedly debugging model with the proposed method. These selected parameters can show the best control performance.

To verify the effectiveness of the proposed control approach, a driving condition of city-bus-route 613 in Chongqing, China, is selected as the simulation condition.

A road section of city-bus-route is extracted from KongGang-Square station to YuBei-Broadcast station that the vehicle speed and the road grade information are shown in Figure 8. It should be noted that, the grade

Table 3 Control parameters

Parameter	Value	Parameter	Value
k_p	0.9	$\bar{k}_3$	7.5
k_i	9.1	χ_1	0.759
k_1	0.62	χ_2	0.317
k_2	11.6	β_1	0.561
k_3	23.5	β_2	0.232
$\bar{k}_1$	0.06	γ_1	0.92
$\bar{k}_2$	1.21	γ_2	0.11

Wang *et al. Chin. J. Mech. Eng.* (2018) 31:58

Page 8 of 11

changes with the distance, so generally the grade-distance curve is used to reflect the grade information of a road section.

4.1 Driving Intention Quantification

To verify the intention recognition, the accelerator pedal position and the actual gear position curve were collected from the driving condition as shown in Figure 9.

As shown in Figure 9, two sections of routes are with fully different driver's maneuvers. The first section from 0 s to 117 s shows the higher acceleration and the larger pedal open than that of the second section from 120 s to 300 s. Therefore, the quantified driving intention is shown as in Figure 10. The result shows that the intention could essentially reflect the actual maneuver. Moreover, the urgent accelerating intention appears in 4.5 s and the rest is the normal accelerating intention. Therefore, the threshold of I_{th} could be selected as 3.2. Because the focus in this paper is the process of PHEB driving mode, two vehicle launch process are extracted from the selected driving condition and the results are shown in Sections 4.2 and 4.3.

4.2 Results under Different Driving Intentions

A clear city-bus-route without traffic jams is simulated in this part. The driver's intention under this condition inclines to drive through this section of road fast, so according to the strategy determination described in Section 3.2, the simulation results are shown in Figure 11.

As shown in Figure 11(a), the results of vehicle speed obtained from the simulation are close to the test data, and the deviation reflects the error between simulation
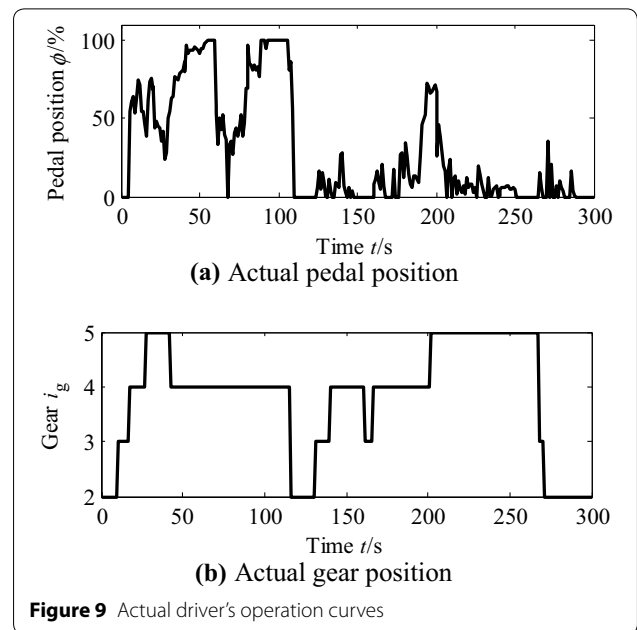
(a) Actual pedal position

(b) Actual gear position

Figure 9 Actual driver's operation curves

model and actual vehicle. With the increasing vehicle speed, the AMT will execute the gear shifting operation in accordance with BGS strategy. The engine torque tracking performance can be ensured, which is shown in Figure 11(c). The designed adaptive robust controller can respond to the demand EM torque quickly and accurately, as shown in Figure 11(d).

A congested city-bus-route is simulated to reflect the driver maneuvers with the intention $I_d(t_{switch}) < I_{th}$. The simulation results are shown in Figure 12. As shown in Figure 12(a), the vehicle speed of simulation is in accordance with the test data, and with the intention of slow driving, Figure 12(c) shows that the engine demand torque is elevated by the generating torque of EM in the driving condition of the low torque demand. In addition, due to the engine response characteristics, the PI controller with the control input of fuel injection cannot eliminate the torque deviation. However, the proposed coupling driving control approach utilizes the EM torque to compensate the above torque deviation, and the good tracking performance is ensured by the designed adaptive robust controller for EM, the effect curves of which is shown in Figure 12(d). Therefore, it can be concluded that the efficient operation of PHEB is ensured. It should be noted that Figure 11 and Figure 12 show two different driving conditions with relevant driving intentions. Under urgent driving condition, the test vehicle uses less time than that under slow driving condition, when it reaches the same speed. Thus, the timeline in Figure 11 shows less than that in Figure 12.

The working points of engine and EM in two different driving intentions are shown in Figure 13. As seen
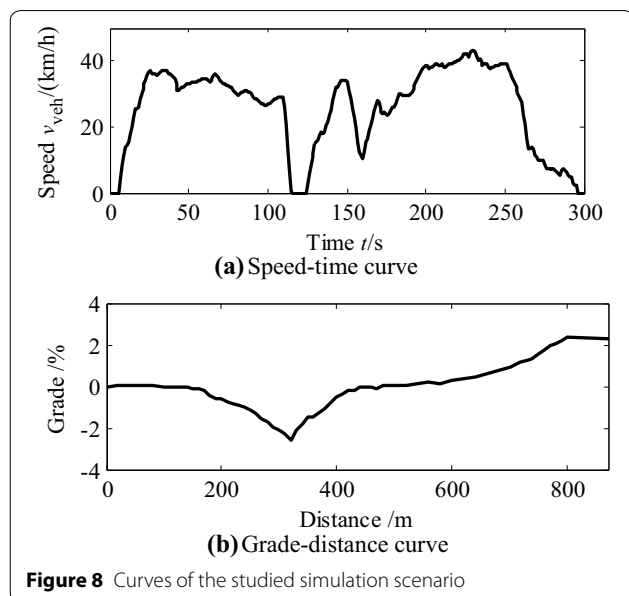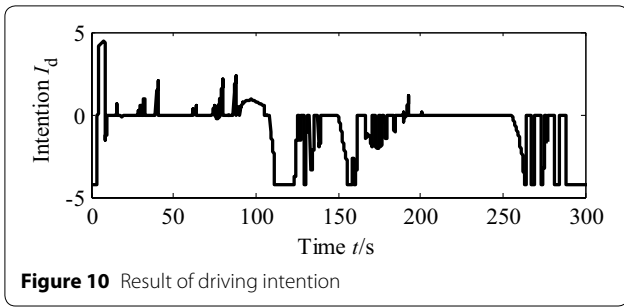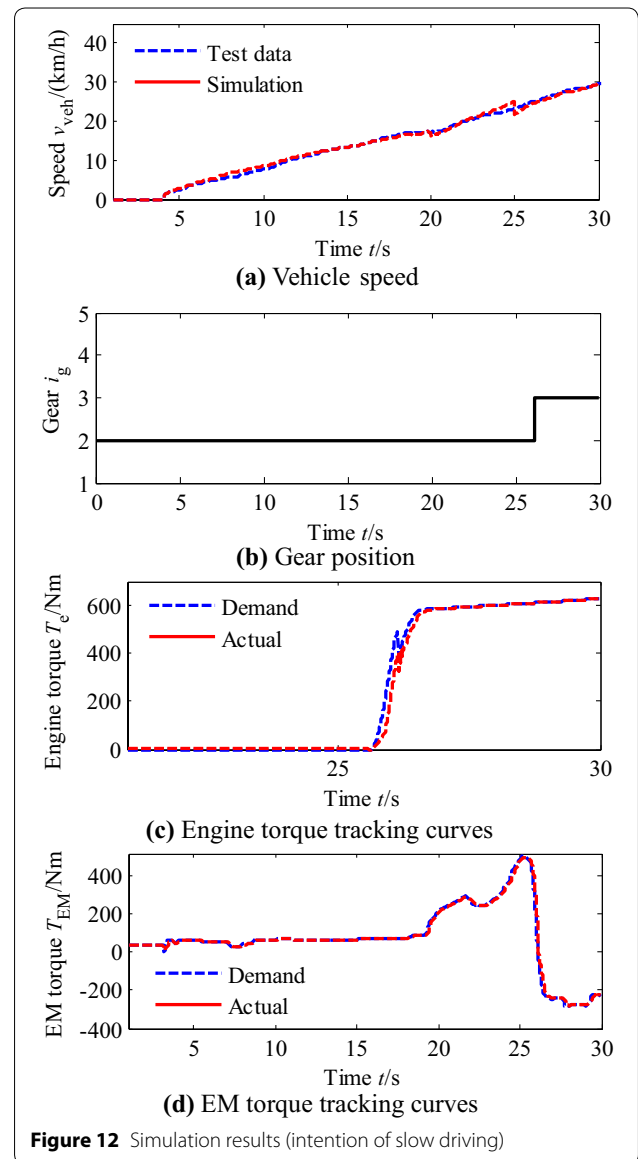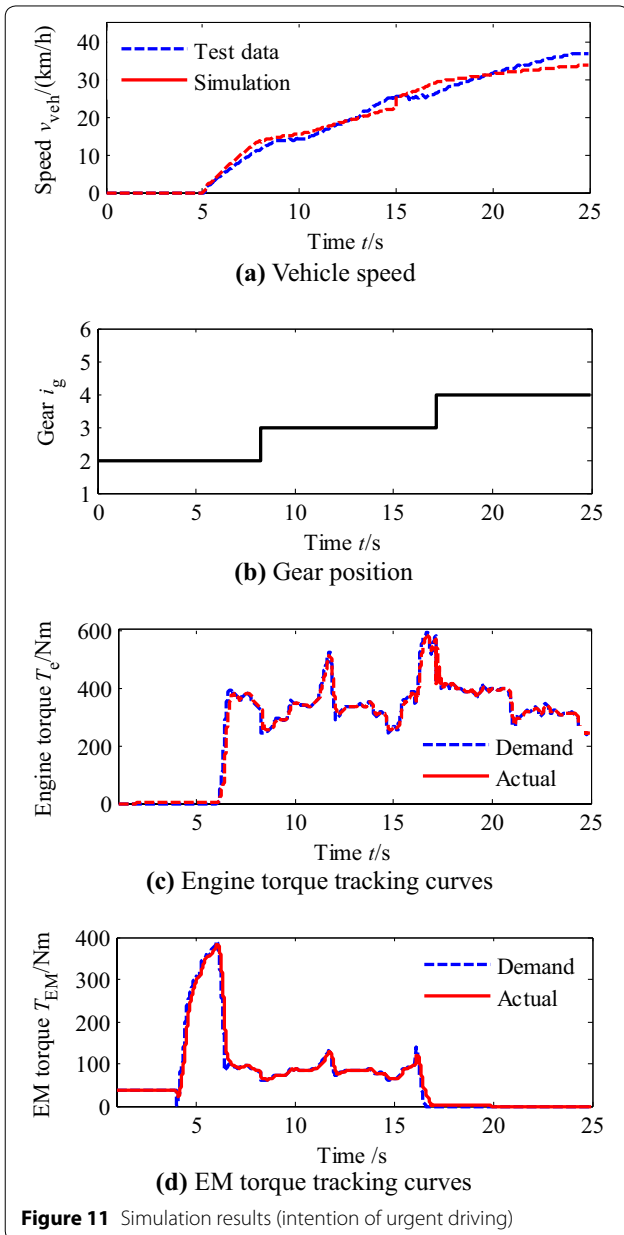
(a) Speed-time curve

(b) Grade-distance curve

Figure 8 Curves of the studied simulation scenario

Wang *et al. Chin. J. Mech. Eng.* (2018) 31:58

Page 9 of 11
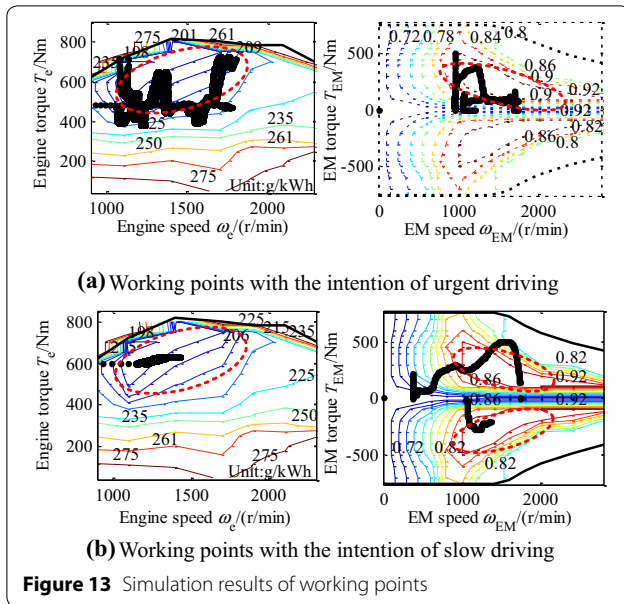

Figure 10 Result of driving intention

in Figure 13, the working areas of engine and EM are improved by the coupling driving mode, especially in engine active charging mode, the working points of engine are moved into its high-efficiency area. To show the improvement of working points more clearly, the areas plot by the red dotted line are defined as the high-efficiency areas of engine and EM. The results show that the working points of engine and EM are greatly improved by the proposed control strategy.

4.3 HIL Test Results

To verify the real-time capability of the proposed control method, the HIL test is carried out. The HIL test platform is shown in Figure 14.

(a) Vehicle speed

(b) Gear position

(c) Engine torque tracking curves

(d) EM torque tracking curves

Figure 11 Simulation results (intention of urgent driving)

(a) Vehicle speed

(b) Gear position

(c) Engine torque tracking curves

(d) EM torque tracking curves

Figure 12 Simulation results (intention of slow driving)

Wang *et al. Chin. J. Mech. Eng.* (2018) 31:58

Page 10 of 11

Figure 13 Simulation results of working points

(a) Working points with the intention of urgent driving

(b) Working points with the intention of slow driving

Figure 15 Test results under Chinese typical urban condition

As shown in Figure 14, the dSPACE real time test system is employed for running the vehicle model. Hybrid control unit (HCU) is the actual controller used in PHEB. The PHEB model built in MATLAB/Simulink are loaded into dSPACE through real time interface (RTI). The C codes of proposed control strategy is generated with the auto code function of real time workshop (RTW), meanwhile, the controller drive program is compiled with the main program in Tasking EDE tool. A PC is employed with control desk to monitor the test operation. The test is carried out in Chinese typical urban condition and its results are shown in Figure 15.

The outstanding vehicle speed tracking performance and the reasonable torque spilt effect can be shown in Figure 15, which proves the proposed control strategy is effective to the real time HIL test. To further show the advantage, a rule-based control strategy is adopted as the baseline strategy, which is commonly used in actual vehicle [19]. The FC and EC represent the fuel consumption
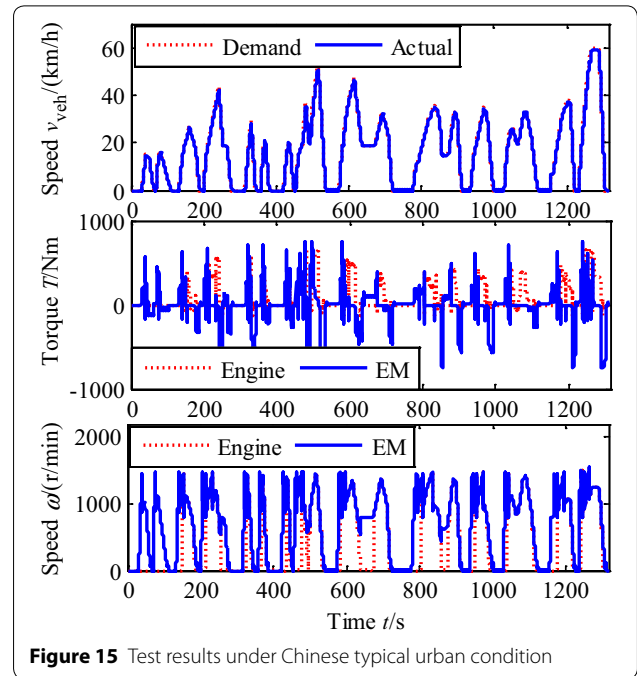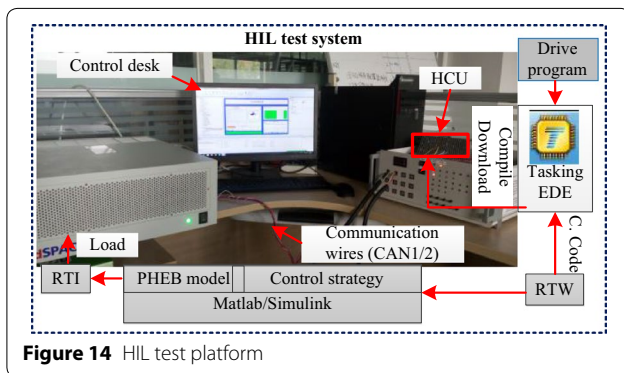
and the electricity consumption, respectively. The average brake specific fuel consumption (BSFC) results reflect the improvement of working points. As shown in Table 4, the fuel consumption improvement is 10.4% under the given driving condition.

5 Conclusions

(1) The driving intention is recognized by the designed fuzzy logic inference.

(2) According to the quantified intention, the mode selection method in the coupling driving mode and AMT gear-shifting strategy given in the strategy determination module by the pre-set threshold.

(3) The adaptive robust controller is designed for EM to ensure the tracking effect with the uncertainties and disturbances.

(4) The proposed control approach could guarantee the torque tracking performance, and the fuel economy can be improved 10.4% through adjusting the engine working points under different driving intentions.

(5) The real time capability of the control approach has been validated by HIL tests. The proposed control method has the potential to apply in the actual vehicle.

Figure 14 HIL test platform

Table 4 Comparison results of two control strategy

Strategy	FC (L)	Improvement (%)	Average BSFC(g/ kWh)
Rule-based	1.25	–	228.23
Proposed	1.12	10.4	204.51

Wang *et al. Chin. J. Mech. Eng.* (2018) 31:58

Page 11 of 11

Author details
[1] Zhongtong Bus Hold Co., Ltd., Liaocheng 252000, Shandong, China. [2] State Key Laboratory of Automotive Safety and Energy, Tsinghua University, Beijing 100084, China.

Authors' Information
Qin-Pu Wang, born in 1964, is the General Manager Assistant at *Zhongtong Bus Hold Co., Ltd., China*. He received his bachelor degree from *Xi'an Highway Institute, China*, in 1984. His research interests include design and manufacture of hybrid electric vehicle. E-mail: QinPu_Wang@163.com.

Chao Yang, born in 1986, is currently a postdoctoral fellow at *State Key Laboratory of Automotive Safety and Energy, Tsinghua University, China*. He received his PhD degree on Control Science and Engineering from *Yanshan University, China*, in 2016. His research interests include energy-efficient control strategy design for hybrid electric vehicles. E-mail: chaoyang1986@tsinghua.edu.cn.

Ya-Hui Liu, born in 1980, is currently an associate professor at *State Key Laboratory of Automotive Safety and Energy, Tsinghua University, China*. He received his bachelor degree from *Jilin University, China*, in 2003 and PhD degree from *Beihang University, China*, in 2009, respectively. His research interests include vehicle system dynamics, steering system and driver-vehicle system. E-mail: liuyahui@tsinghua.edu.cn.

Yuan-Bo Zhang, born in 1990, is currently working at *State Key Laboratory of Automotive Safety and Energy, Tsinghua University, China*. His research interests include regenerative braking control strategy for electrified vehicles. E-mail: yuanbzhang@163.com.

Publisher's Note
Springer Nature remains neutral with regard to jurisdictional claims in published maps and institutional affiliations.

References
[1] Yong Sun, Zi-Lin Ma, Gong-You Tang, et al. Estimation method of state-of-charge for lithium-ion battery used in hybrid electric vehicles based on variable structure extended kalman filter. *Chinese Journal of Mechanical Engineering*, 2016, 29(4): 717–726.

[2] Chao Yang, Liang Li, Si-Xiong You, et al. Cloud computing-based energy optimization control framework for plug-in hybrid electric bus. *Energy*, 2017, 125: 11–26.

[3] Liang Li, Si-Xiong You, Chao Yang, et al. Driving-behavior-aware stochastic model predictive control for plug-in hybrid electric buses. *Applied Energy*, 2016, 162: 868–879.

[4] Marcello Canova, Yann Guezennec, Steve Yurkovich. On the control of engine start/stop dynamics in a hybrid electric vehicle. *ASME Transactions, Journal of Dynamic System, Measurement, and Control*, 2009, 131(12), 061005: 1–12.

[5] Zheng Chen, Bing Xia, Chenwen You, et al. A novel energy management method for series plug-in hybrid electric vehicles. *Applied Energy*, 2015, 145: 172–179.

[6] Chao Yang, Jian Song, Liang Li, et al. Economical launching and accelerating control strategy for a single-shaft parallel hybrid electric bus. *Mechanical Systems and Signal Processing*, 2016, 76-77: 649–664.

[7] Tian-Heng Feng, Lin Yang, Qing Gu, et al. A supervisory control strategy for plug-in hybrid electric vehicles based on energy demand prediction and route preview. *IEEE Transactions on Vehicular Technology,* 2015, 64(5): 1691–1770.

[8] Hong-Cai Li, Qing-Dong Yan, Chang-Le Xiang, et al. Analysis method and principle of dual-mode electro-mechanical variable transmission program. *Chinese Journal of Mechanical Engineering*, 2012, 25(3): 524–529.

[9] Wei-Da Wang, Li-Jin Han, Chang-Le Xiang, et al. Synthetical efficiency-based optimization for the power distribution of power-split hybrid electric vehicles. *Chinese Journal of Mechanical Engineering*, 2014, 27(1): 58–68.

[10] Dongsuk Kum, Huei Peng, Norman Bucknor. Control of engine-starts for optimal drivability of parallel hybrid electric vehicles. *ASME Transactions, Journal of Dynamic System, Measurement, and Control*, 2014, 135(3), 021020: 1–10.

[11] Liang Li, Chao Yang, Ya-Hui Zhang, et al. Correctional DP-based energy management strategy of plug-in hybrid bus for city-bus-route. *IEEE Transactions on Vehicular Technology*, 2015, 64(7): 2792–2803.

[12] Chan-Chiao Lin, Huei Peng, Jessy-W. Grizzle et al. Power management strategy for a parallel hybrid electric truck. *IEEE Transactions on Control Systems Technology*, 2003, 11(6): 839–849.

[13] Chao Yang, Siyu Du, Liang Li, et al. Adaptive real-time optimal energy management strategy based on equivalent factors optimization for plug-in hybrid electric vehicle. *Applied Energy*, 2017, 203: 883–896.

[14] Bo Geng, James-K. Mills, Dong Sun. Energy management control of microturbine-powered plug-in hybrid electric vehicles using the telemetry equivalent consumption minimization strategy. *IEEE Transactions on Vehicular Technology*, 2011, 60(9): 4238–4248.

[15] Feng-Jun Yan, Jun-Min Wang, Kai-Sheng Huang. Hybrid electric vehicle model predictive control torque-split strategy incorporating engine transient characteristics. *IEEE Transactions on Vehicular Technology*, 2012, 61(6): 2458–2467.

[16] Li Chen, Gang Xi, Jing Sun. Torque coordination control during mode transition for a series-parallel hybrid electric vehicle. *IEEE Transactions on Vehicular Technology*, 2012, 61(7): 2936–2949.

[17] K Koprubasi, E R Westervelt, G Rizzoni. Toward the systematic design of controllers for smooth hybrid electric vehicle mode changes. *Proceedings of the 2007 American Control Conference*, 2007: 2985–2990.

[18] Hyunsup Kim, Jihun Kim, Hyeongcheol Lee. Mode transition control using disturbance compensation for a parallel hybrid electric vehicle. *Proceedings of the Institution of Mechanical Engineers, Part D: Journal of Automobile Engineering*, 2012, 225: 125–150.

[19] Lin He, Tie-Long Shen, Liang-Yao Yu, et al. A model-predictive-control-based torque demand control approach for parallel hybrid powertrains. *IEEE Transactions on Vehicular Technology*, 2013, 62(3): 1041–1052.

[20] Stefano Cordiner, Sergio Galeani, Francesco Mecocci, et al. Torque set-point tracking for parallel hybrid electric vehicles using dynamic input allocation. *IEEE Transactions on Control Systems Technology*, 2014, 22(5): 2007–2015.

[21] V T Minh, A A Rashid. Modeling and model predictive control for hybrid electric vehicles. *International Journal of Automotive Technology*, 2012, 13(3): 477–485.

[22] Metin Gokasan, Seta Bogosyan, D J Goering. Sliding mode based power-train control for efficiency improvement in series hybrid-electric vehicles. *IEEE Transactions on Power Electronics*, 2006, 21(3): 779–790.

[23] Chao Yang, Xiao-Hong Jiao, Liang Li, et al. Electromechanical coupling driving control for single-shaft parallel hybrid powertrain. *SCIENCE CHINA Technological Sciences*, 2014, 57(3): 541–549.

[24] Chao Yang, Xiao-Hong Jiao, Liang Li, et al. Robust coordinated control for hybrid electric bus with single-shaft parallel hybrid powertrain. *IET Control Theory and Application*, 2015, 9(2): 270–282.